arXiv:1408.0212v2 [nlin.PS] 8 Dec 2014

Quantization of β-Fermi-Pasta-Ulam Lattice with Nearest and Next-nearest Neighbour Interactions

Aniruddha Kibey[a], Rupali Sonone[a], Bishwajyoti Dey[1a], J. Chris Eilbeck[b]

[a] *Department of Physics, University of Pune, Pune - 411007, India*
[b] *Department of Mathematics and Maxwell Institute, Heriot-Watt University, Riccarton, Edinburgh, EH14 4AS, UK*

Abstract

We quantize the β-Fermi-Pasta-Ulam (FPU) model with nearest and next-nearest neighbor interactions using a number conserving approximation and a numerically exact diagonalization method. Our numerical mean field bi-phonon spectrum shows excellent agreement with the analytic mean field results of Ivić and Tsironis ((2006) Physica D 216 200), except for the wave vector at the midpoint of the Brillouin zone. We then relax the mean field approximation and calculate the eigenvalue spectrum of the full Hamiltonian. We show the existence of multi-phonon bound states and analyze the properties of these states by varying the system parameters. From the calculation of the spatial correlation function we then show that these multi-phonon bound states are particle like states with finite spatial correlation. Accordingly we identify these multi-phonon bound states as the quantum equivalent of the breather solutions of the corresponding classical FPU model. The four-phonon spectrum of the system is then obtained and its properties are studied. We then generalize the study to an extended range interaction and consider the quantization of the β-FPU model with next-nearest-neighbor interactions. We analyze the effect of the next-nearest-neighbor interactions on the eigenvalue spectrum and the correlation functions of the system.

[1] bdey@physics.unipune.ac.in
Accepted in Physica D

1. Introduction

The Fermi-Pasta-Ulam (FPU) model marked the beginning of the field of nonlinear dynamics. It was initially introduced to examine the possibility of equipartition of energy in a chain of coupled nonlinear oscillators in the thermodynamic limit [1]. Since then this model has been used to study many important problems in non-equilibrium statistical mechanics, in particular heat conduction in a 1D chain [2]. Other interesting aspects of the dynamics of FPU lattice are the occurrence of intrinsic localized modes (ILMs) or discrete breathers (DBs). ILMs or DBs are time periodic and spatially localized solutions of the nonlinear lattice and occur due to the balance between nonlinearity and discreteness. ILMs have been experimentally observed in various physical systems ranging from lattice vibrations in crystals and magnetic solids, Josephson junction, photonic crystals etc. ILMs have been used for modeling observed physical processes in polymers and bio-polymers such as, folding in the polypeptide chain, targeted breaking of chemical bonds, charge and energy transport in conducting polymers etc., see [3] for a review. MacKay and Aubry rigorously established the existence of breather excitations in lattices under a wide range of conditions [4]. Exact compact breather-like solutions of the two-dimensional FPU lattice were also obtained [5]. The effect of long-range interactions, the geometry of the chain and nonlinear dispersion on the dynamics of breathers in two-dimensional FPU lattices, and the usefulness of these solutions for energy localization and transport in various physical systems are reported in [6].

It is well known that the integrable classical field equations, such as the sine-Gordon equation [7], nonlinear Schrodinger equation [8] and modified and extended KdV equations [9], support classical breather solutions which are a bound state of soliton and antisoliton pair with continuum classical spectrum. On the other hand the Bohr-Sommerfeld semi-classical quantization for classical breathers shows discrete excitations which are bound states of small-amplitude wave excitations [10]. Faddeev and Korepin, while studying the quantum theory of solitons for integrable systems, showed that the breathers of classical integrable field equations are indeed multi-phonon bound states [11]. These studies led to the question of the nature of quantum breathers in nonlinear lattices. Even though there has been some studies along this line for the nonlinear Klein-Gordon lattice and discrete nonlinear Schrodinger equation [12], not much is known about the nature of quantum breathers in FPU lattice model. The problem of quantization of classical

discrete breathers in FPU model is difficult to solve exactly due to the non-local and anharmonic nature of interactions in the model, which give rise to number non conserving terms in the Hamiltonian. Various truncation methods have been used to obtain the approximate eigenspectra of the system. Ivić and Tsironis [13] studied analytically the discrete breather quantization problem in a β-FPU lattice by truncating the Hamiltonian to include only number conserving terms, and analyzed the bi-phonon sector of the model under the mean field approximation. The number conserving approximation is equivalent to rotating wave approximation used for studying the classical discrete breathers. Ivić and Tsironis showed the occurrence of bi-phonons of two types, the on-site and nearest neighbor site and interpreted these bi-phonons as the quantum counterparts of the classical FPU discrete breathers. Xin-Guang and Yi [14] showed the occurrence of a third type, a mixed bi-phonon state, in a β-FPU model from their numerical exact diagonalization study. However they did not study the four-phonon eigenspectra, the correlation functions, or the effect of the long range interactions on the eigenspectra of the system. Riseborough studied analytically the quantized breather problem on FPU lattice in the two-phonon sector by truncating the equation of motion of the two-phonon propagator, using the ladder approximation in which the single-phonon self-energies are neglected [15]. From the poles of the two-phonon propagator he obtained isolated frequencies which represent the discrete dispersion relations for the collective breather excitations. Recently the bound states of four bosons in the quantum β-FPU lattice have been reported in [16]. However, they did not study the effect of the long range interactions and the spatial correlation functions of the system.

In this paper we study this problem by numerically exact diagonalization using the number state basis and including only number conserving terms. The numerically exact diagonalization method has been successfully applied to the Bose-Hubbard and modified Bose-Hubbard Hamiltonians ([17]-[19]). The purposes of our studies are manifold: (i) to check how the analytical results of Ivić and Tsironis [13], which are obtained under the mean field approximation and in the large eigenvalue limit, compare with the numerically exact diagonalization mean field results; (ii) to go beyond the mean field approximation and obtain numerical eigenspectra of the system; (iii) to study the problem for the higher quanta sector; (iv) to calculate the spatial correlation functions to identify and establish the main characteristics of the spatial localization of the discrete breathers in the quantum excitation spectrum and (v) to generalize the problem to examine the effect of

increasing range of interactions, for which we study the β-FPU model with next-nearest-neighbor (NNN) interactions. Interestingly, we find that the analytical mean field results in the large eigenvalue limit of Ivić and Tsironis [13] agree very well with our numerically exact diagonalization results. We also find that the eigenspectra for the complete Hamiltonian (beyond the mean field case) is quite different as compared to that of the mean field case. Contrary to the mean field case, the nearest neighbor site bi-phonon mode do not get distinctly separated from the quasi-continuum band. This is in agreement with [14]. The four-phonon spectrum shows that the states which belong to the free phonon band now split into several bands due to the effect of nonlinearity. The isolated band corresponds to discrete breathers. A similar splitting of bands for the higher quanta sector of the Klein Gordon type nonlinear lattice has been reported by Wang et al. [20] from their numerically exact diagonalization calculations using an Einstein phonon basis. The spatial correlation functions for the on-site bi-phonon, as well as the four-phonon states, show strong localization at particular sites. This shows the particle like nature of the states which identifies these states with corresponding classical on-site discrete breathers. Similarly, the inclusion of the NNN interaction in the β-FPU model changes the lattice periodicity and its effect on the eigenspectra is clearly seen.

It may be noted that the number conserving approximation cannot be used for α-Fermi-Pasta-Ulam lattice. This is because the cubic interaction terms in the α-Fermi-Pasta-Ulam Hamiltonian are all number non-conserving.

It is appropriate to mention here that quantum breather excitations have been seen in experiments as sharp discrete peaks in the excitation spectrum of the ionic crystal NaI [21], as bound states of up to seven phonons in PtCl [22], as two-phonon bound states in the infrared absorption spectra of CO_2 crystals [23], as a carrier of vibrational energy without dispersing for over more than 10^7 unit cells of layered crystal muscovite [24] etc. See [12] for more details.

The plan of the paper is as follows: In Sec. 2 we describe the Hamiltonian of the β-Fermi-Pasta-Ulam lattice and the quantization scheme. We write the Hamiltonian in terms of the phonon creation and annihilation operators within the number conserving approximation. In section 3 we describe the computational method. In section 4 we write the Hamiltonian under the mean field approximation. In section 5 we write the complete and mean field Hamiltonians for NNN interaction in terms of the phonon creation and

annihilation operators and in section 6 we present the results and discussion. Finally we conclude in section 7.

2. The β-Fermi-Pasta-Ulam model and its quantization

The Hamiltonian for the classical one dimensional β-FPU model for N identical oscillators in a periodic lattice is given by [13]

$$H = \sum_j \left[\frac{p_j^2}{2m} + \frac{\alpha}{2} (x_j - x_{j-1})^2 + \frac{\beta}{4} (x_j - x_{j-1})^4 \right] \tag{1}$$

where α is the nearest-neighbor harmonic force constant and β is the anharmonic force constant. The position and momentum operators of the j-th particle can be written in terms of the phonon creation and annihilation operators as

$$\begin{aligned} x_j &= \sqrt{\frac{\hbar}{2m\omega}} \left(a_j^\dagger + a_j \right) \\ p_j &= i\sqrt{\frac{\hbar}{2m\omega}} \left(a_j^\dagger - a_j \right) \end{aligned}$$

The creation and annihilation operators follow the commutation relations given by $[a_j, a_k^\dagger] = \delta_{jk}$, and $[a_j, a_k] = [a_j^\dagger, a_k^\dagger] = 0$. Retaining only the number conserving terms, by virtue of the lattice periodicity and assuming $N \to \infty$,where N is the number of lattice sites, the Hamiltonian can be written as [13]

$$\begin{aligned} H &= \epsilon_o + \hbar\bar{\omega} \sum_j a_j^\dagger a_j - J' \sum_j a_j^\dagger \left(a_{j+1} + a_{j-1} \right) \\ &\quad + B \sum_j \left[a_j^{\dagger 2} a_j^2 + \frac{1}{2} a_j^{\dagger 2} \left(a_{j+1}^2 + a_{j-1}^2 \right) \right] \\ &\quad + B \sum_j \sum_{s=\pm 1} \left[a_j^\dagger a_j a_{j+s}^\dagger a_{j+s} - \left(a_j^{\dagger 2} a_j a_{j+s} + \text{h.c.} \right) \right] \end{aligned} \tag{2}$$

where

$$\epsilon_0 = \frac{\hbar\omega N}{2} \left(1 + \frac{3\beta}{2\alpha} \left(\frac{\hbar}{2M\omega} \right) \right), \tag{3}$$

$$\bar{\omega} = \omega \left(1 + \frac{3\beta}{\alpha} \left(\frac{\hbar}{2M\omega} \right) \right), \tag{4}$$

$$J' = \alpha \left(\frac{\hbar}{2M\omega}\right)\left(1+\frac{3\beta}{\alpha}\frac{\hbar}{M\omega}\right), \quad (5)$$

$$B = 3\beta\left(\frac{\hbar}{2M\omega}\right)^2 \quad (6)$$

3. The Computational Method

In Eqs. (1) and (2) we assume that the number of lattice sites is infinite, but in practice we can work with a finite number of sites. To simulate the infinite lattice, with finite number of sites, we incorporate the periodic boundary conditions (ring geometry). We consider a system with f lattice sites. Since we use the number conserving approximation, the Hamiltonian operator commutes with the number operator $\hat{N} = \sum_{j=1}^{f} a_j^\dagger a_j$, where $j = 1, 2, 3, \ldots, f$ are lattice points. This implies that the operators H and $\hat{N}$ have simultaneous eigenstates. Hence we can block-diagonalize the Hamiltonian matrix using simultaneous eigenstates of H and $\hat{N}$ as

$$H = \begin{pmatrix} H_0 & 0 & 0 & \cdots \\ 0 & H_1 & 0 & \cdots \\ 0 & 0 & H_2 & \cdots \\ \vdots & \vdots & \vdots & \ddots \end{pmatrix} \quad (7)$$

where each block H_m describes states with m bosons. This greatly simplifies the calculations. Because of this block diagonal structure, it is possible to deal with each block independently [17, 18]. For example in the paper we have calculated the energy spectrum for two quanta sector and four quanta sector. This corresponds to the blocks H_2 (Section 6.1) and H_4 (Section 6.2) respectively.

In the number state representation, the basis state is denoted by $|\psi_n\rangle = [n_1, n_2, ...n_f]$, where n_j denotes the number of quanta (bosons) at lattice site j. For example [1 1 0 0], represents a two quanta state with four lattice sites, with one boson each at the first and the other at the second lattice sites and no bosons at the other two lattice sites, $N = \sum_j n_j$. For m quanta and f sites there are $\frac{(m+f-1)!}{m!(f-1)!}$ possible states [17, 18]. For example for a 1D periodic lattice of $f = 3$ sites and $m = 2$ bosons, there are 6 possible states [2 0 0], [0 2 0], [0 0 2], [1 1 0], [0 1 1], and [1 0 1] and therefore H_2 for this particular case is 6×6 matrix.

To generate the Hamiltonian matrix, we make use of a hash table [25]. To generate the label for each state, we assign a weight to each lattice point as $w_j = \sqrt{p_j}$ where p_j is the j^{th} prime. The label for a state is given by, $\sigma([state]) = \sum_{j=1}^{j=f} w_j n_j$, where n_j is the number of quanta at the j^{th} lattice point. Use of the hash table considerably reduces the number of operations needed to generate the Hamiltonian matrix.

Further, under the periodic boundary conditions, the Hamiltonian is invariant under the action of the translation operator $\hat{T}$. Hence we can use the translation invariant states to further block-diagonalize each block of the Hamiltonian matrix [17, 18]. The number of translation invariant states ($\mathcal{N}$) for the system is given by [17, 18]

$$\mathcal{N} = \frac{(m+f-1)!}{m!f!}$$

Hence for 2 quanta and 3 sites, the number of translation invariant states is 2 for each value of k. The two translation invariant states of a system with two quanta and three lattice sites are given by

$$|\psi_1\rangle = [2\,0\,0] + t\,[0\,2\,0] + t^2\,[0\,0\,2] \quad (8)$$

$$|\psi_2\rangle = [1\,1\,0] + t\,[0\,1\,1] + t^2\,[1\,0\,1] \quad (9)$$

where t=e^{ik}, with corresponding k values $0, \pm 2\pi/3$, so that $t^3 = 1$. Thus we can further block-diagonalize H_2 into three 2×2 blocks $H_{2,k}$ using the translationally invariant states. The eigenvalues and eigenvectors of each of the 2×2 blocks can be calculated separately. This greatly reduces the memory requirement of each calculation. The allowed values of k for a lattice with f sites are $k = \frac{2\pi}{f}\nu$, where $\nu = 0,\ \pm 1,\ \pm 2, ... \pm (\frac{f}{2} - 1),\ \pm\frac{f}{2}$ for f even and $\nu = 0,\ \pm 1,\ \pm 2, ... \pm \frac{f-1}{2}$ for f odd [17].

The number of invariant states increase rapidly with increase in the number of quanta and also with the number of lattice points. An arbitrary state vector of the system is given by

$$|\Psi\rangle = \sum_j C_j\,|\psi_j\rangle \quad (10)$$

The normalization condition $\langle\Psi|\Psi\rangle = 1$ gives $\sum_j |C_j|^2 = 1$.

Exact numerical diagonalization, using the LAPACK package [26], is then used to calculate the eigenvalues and eigenvectors of the Hamiltonian matrix for the m-quanta sector on a lattice with f sites. To plot

the energy spectrum we have considered $\epsilon(k) = (E_j(k) - 2\hbar\omega)/2J'$, where $E_j(k)$ are the eigenvalues of the Hamiltonian matrix. The k dependence of the energy $E_j(k) = \langle\Psi|H|\Psi\rangle$ comes from the $t = e^{ik}$ dependence of the general state vector $|\Psi\rangle$ of the system (Eq.(10)), , with $k = \frac{2\pi\nu}{f}$, where $\nu = 0, \pm1, \pm2, \ldots, \pm(f-1)/2$, through the translation invariant states $|\psi_1\rangle$ and $|\psi_2\rangle$ (Eqs.(8 and 9)).

Spatial correlation function: To identify breathers in the eigenspectra so obtained, we calculate the spatial correlation function to establish the main characteristic of spatial localization. The spatial correlation of the displacements at sites separated by n-lattice spacings is given by the expression [20]

$$f_\alpha(j - j') = \langle\alpha|\, \hat{x_{j'}}\, \hat{x_j}\, |\alpha\rangle \tag{11}$$

where $|\alpha\rangle$ denotes the eigenvector of the Hamiltonian and x_j is the displacement at the j^{th} site. Using the phonon creation and annihilation operators and the number conserving approximation, we can write the above correlation function as

$$f_\alpha(j - j') = \frac{\hbar}{2m\omega}\langle\alpha|\left(a^\dagger_{j'}a_j + a_{j'}a^\dagger_j\right)|\alpha\rangle \tag{12}$$

4. Mean field approximation :

The last two terms in Eq. (2) describes bivibron tunneling [13]. These terms may be treated within the mean field approximation as an effective single vibron intersite tunneling and written as $2\langle a^\dagger a\rangle \sum_j a^\dagger_j(a_{j+1} + a_{j-1})$, where $\langle a^\dagger a\rangle$ denote the expectation value of the number operator $a^\dagger a$ in an arbitrary state of the system. The details are given in the Appendix. These two bivibron tunneling terms can now be added to the single vibron tunneling terms (3rd term in Eq. (2)) to get the mean field Hamiltonian with effective parameter $J = J' + 2B\langle a^\dagger a\rangle$ [13]. The effective Hamiltonian takes the form

$$\begin{aligned} H_{\rm MF} &= \epsilon_o + \hbar\bar{\omega}\sum_j a^\dagger_j a_j - J\sum_j a^\dagger_j\left(a_{j+1} + a_{j-1}\right) \\ &\quad + B\sum_j\left[a^{\dagger 2}_j a^2_j + \frac{1}{2}a^{\dagger 2}_j\left(a^2_{j+1} + a^2_{j-1}\right)\right] \\ &\quad + B\sum_j\sum_{s=\pm1} a^\dagger_j a_j a^\dagger_{j+s}a_{j+s}, \end{aligned} \tag{13}$$

Thus mean field approach approximates the direct bivibron tunneling process by effective single vibron tunneling. This allows approximate analytic solution of the problem as shown in [13].

5. The Fermi-Pasta-Ulam lattice with nearest and next-nearest-neighbor interaction

Here we generalize the problem by including next-nearest neighbor interactions to examine the effect of the long-range interaction on the energy spectrum and correlation function of the system. Physical systems such as polymers and biopolymers contain various charged groups which interact with a long-range Coulomb force. Similarly, the excitation transfer in molecular crystals and energy transport in biopolymers are due to the transition dipole-dipole interactions. Several studies of the classical discrete breathers in presence of long-range interactions in one-dimensional chain have been reported in the literature, for details see [6]. Here we consider the one-dimensional β- FPU chain with nearest and next-nearest neighbor interactions. The classical Hamiltonian can be written as

$$\begin{aligned} H &= \sum_j \left[\frac{p_j^2}{2m} + \frac{\alpha}{2}\left(x_j - x_{j-1}\right)^2 + \frac{\alpha_1}{2}\left(x_j - x_{j-2}\right)^2 \right. \\ &\qquad \left. + \frac{\beta}{4}\left(x_j - x_{j-1}\right)^4 + \frac{\beta_1}{4}\left(x_j - x_{j-2}\right)^4 \right] \end{aligned}$$

Retaining only the number conserving terms and by virtue of the lattice periodicity, the Hamiltonian can be written as

$$\begin{aligned} H &= \epsilon_o + 2\hbar\bar{\omega}\sum_j a_j^\dagger a_j - J'\sum_j a_j^\dagger\left(a_{j+1}+a_{j-1}\right) \\ &+B\sum_j\left[a_j^{\dagger 2}a_j^2+\tfrac{1}{2}a_j^{\dagger 2}\left(a_{j+1}^2+a_{j-1}^2\right)\right] \\ &+B\sum_j\sum_{s=\pm 1}\left[a_j^\dagger a_j a_{j+s}^\dagger a_{j+s}-(a_j^{\dagger 2}a_j a_{j+s}+\text{h.c.})\right] \\ &-J_1'\sum_j a_j^\dagger\left(a_{j+2}+a_{j-2}\right) \\ &+B_1\sum_j\left[a_j^{\dagger 2}a_j^2+\tfrac{1}{2}a_j^{\dagger 2}\left(a_{j+2}^2+a_{j-2}^2\right)\right] \\ &+B_1\sum_j\sum_{s=\pm 2}\left[a_j^\dagger a_j a_{j+s}^\dagger a_{j+s}-(a_j^{\dagger 2}a_j a_{j+s}+\text{h.c.})\right] \end{aligned} \tag{14}$$

where the J' and B are given by Eqs. (5) and (6) respectively and the J_1' and B_1 are given by

$$\begin{aligned} J_1' &= \alpha_1\left(\frac{\hbar}{2M\omega}\right)\left(1+\frac{3\beta_1}{\alpha_1}\frac{\hbar}{M\omega}\right), \\ B_1 &= 3\beta_1\left(\frac{\hbar}{2M\omega}\right)^2 \end{aligned}$$

Using the mean field approximation as mentioned above, the mean field Hamiltonian for the β-FPU lattice with NN and NNN interactions in a given quanta sector can be written as

$$\begin{aligned} H &= \epsilon_o + 2\hbar\bar{\omega}\sum_j a_j^\dagger a_j \\ &-(J'+2B\sum_j\langle a^\dagger a\rangle)\sum_j a_j^\dagger\left(a_{j+1}+a_{j-1}\right) \\ &+B\sum_j\left[a_j^{\dagger 2}a_j^2+\tfrac{1}{2}a_j^{\dagger 2}\left(a_{j+1}^2+a_{j-1}^2\right)\right] \end{aligned}$$

$$
\begin{aligned}
&+B\sum_{j}\sum_{s=\pm1} a_j^{\dagger}a_j a_{j+s}^{\dagger}a_{j+s} \\
&-(J_1' + 2B_1\left\langle a^{\dagger}a\right\rangle)\sum_{j} a_j^{\dagger}\left(a_{j+2}+a_{j-2}\right) \\
&+B_1\sum_{j}\left[a_j^{\dagger 2}a_j^2 + \tfrac{1}{2}a_j^{\dagger 2}\left(a_{j+2}^2+a_{j-2}^2\right)\right] \\
&+B_1\sum_{j}\sum_{s=\pm2} a_j^{\dagger}a_j a_{j+s}^{\dagger}a_{j+s} \qquad (15)
\end{aligned}
$$

6. Results and Discussions

6.1. ***Two quanta sector***

We first consider the discrete breather bands at the second quantum level ($m = 2$) or in the two-quanta sector. This corresponds to the block H_2 of the Hamiltonian matrix (Eq.(7)). The $m = 2$ state is obtained by operating two phonon creation operators on the ground state of the system. For example, for a lattice with three sites the $m = 2$ state is given by the (Eq.(10)) along with (Eqns.(8 and 9)). For details see (Eq.(13)) of [13]. We have considered a lattice of 101 lattice sites. As mentioned above, for odd number of sites the allowed maximum value of $k = \pm\frac{2\pi}{f}\frac{(f-1)}{2} \sim \pm\pi$ for large f. Therefore we plot the eigenspectrum for $-1 \leq \frac{k}{\pi} \leq +1$.

To begin with, we compare our numerical exact diagonalization mean field result with the approximate analytical mean field result of Ivić and Tsironis [13] for the two-quanta sector. For easy reference, we have reproduced the mean field results of [13] as Fig. 1(e). Fig. 1(a) shows our numerical results obtained for the choice of parameter value $2B/J = -2$ which is same as the parameter value considered in [13] (shown in Fig. 1.(e) by red lines). Fig. 1.(e) shows that the two bands corresponding to the on-site and nearest-neighbor (off-site) biphonon states (continuous and dotted red curves respectively) cross each other at $k/\pi = \pm\frac{1}{2}$. Ivić and Tsironis attributed this behavior to the approximate nature of their analytical calculations and suggested to verify this fact through numerically exact diagonalization method. As mentioned in the introduction, one of the motivations of our present work is to compare the analytic mean field results of Ivić and Tsironis with our exact diagonalization results. From our study we find that that the crossings of the two bound biphonon bands at $k/\pi = \pm\frac{1}{2}$ as obtained by Ivić and Tsironis is indeed an artifact of the approximate nature of their analytic calculations,

as our numerically exact diagonalization results (Fig. 1(a)) shows no such band crossings. Fig. 1(b) shows the energy spectrum for the complete Hamiltonian where the parameter $J^{'}$ is related to mean field parameters J in Fig. 1(a) by the relation $J = J^{'} + 2B\langle a^{\dagger}a\rangle$. Fig. 1.(c) is the numerical mean field result for another set of parameter value $2B/J = -20$. This large value of the parameter $(2B/J)$ shows the separation of the two bound states very clearly (shown by the red lines). Again, our numerical mean field results do not show any band crossing at $k/\pi = \pm\frac{1}{2}$. Fig. 1.(d) shows the eigenspectra for the complete Hamiltonian where the parameter $J^{'}$ is related to mean field parameters J in Fig. 1(c) by the relation $J = J^{'} + 2B\langle a^{\dagger}a\rangle$. Fig. 1.(f) shows the results only for the complete Hamiltonian. This figure is plotted for large value of the parameter $|B| = 1.2857$ to show larger band separation between the lowest two bands. The biphonon spectrum for repulsive interaction $B > 0$ is exactly symmetric to the one for attractive interaction $B < 0$, but *above* the free two-phonon band (not shown in the figure). However, contrary to the mean field case, the off-site biphonon mode is not distinctly separated from the quasi-continuum band even for large values of $2B/J'$. This is in agreement with the results of Xin-Guang and Yi [14]. To see why the off-site biphonon mode is not distinctly separated from the quasi-continuum band, we consider the matrix obtained for the two quanta mean-field Hamiltonian (Eq. (13)) given by

$$H_{\mathrm{MF}}(k) = \begin{pmatrix} D & E_+ & 0 & 0 & \cdots & \cdots & 0 & 0 \\ E_- & H & F_+ & 0 & \cdots & \cdots & 0 & 0 \\ 0 & F_- & 2 & F_+ & \cdots & \cdots & \vdots & 0 \\ \vdots & 0 & F_- & \ddots & \cdots & \cdots & 0 & \\ \vdots & \vdots & \vdots & \vdots & \ddots & \cdots & \vdots & \vdots \\ \vdots & \vdots & \vdots & \vdots & \vdots & \ddots & F_+ & 0 \\ 0 & 0 & 0 & \cdots & \cdots & F_- & 2 & F_+ \\ 0 & 0 & 0 & \cdots & \cdots & 0 & F_- & G \end{pmatrix}$$

where $D(k) = 2\hbar\omega + 2B(1+\cos(k))$, $E_{\pm}(k) = -\sqrt{2}(1+\exp(\pm ik))J$, $F_{\pm}(k) = J(1+\exp(\pm ik))$, $G(k) = -2J\cos(\frac{1}{2}(f+1)k)$ and $H = 2(1+B)$. Similarly,

the matrix obtained for the complete Hamiltonian (Eq. (2)) is

$$H_{comp}(k) = \begin{pmatrix} D' & E'_+ & 0 & 0 & \cdots & \cdots & 0 & 0 \\ E'_- & H' & F'_+ & 0 & \cdots & \cdots & 0 & 0 \\ 0 & F'_- & 2 & F'_+ & \cdots & \cdots & \vdots & 0 \\ \vdots & 0 & F'_- & \ddots & \cdots & \cdots & \cdots & 0 \\ \vdots & \vdots & \vdots & \vdots & \ddots & \cdots & \vdots & \vdots \\ \vdots & \vdots & \vdots & \vdots & \vdots & \ddots & F'_+ & 0 \\ 0 & 0 & 0 & \cdots & \cdots & F'_- & 2 & F'_+ \\ 0 & 0 & 0 & \cdots & \cdots & 0 & F'_- & G' \end{pmatrix}$$

where $D'(k) = 2\hbar\omega + 2B(1+\cos(k))$, $E'_{\pm}(k) = -\sqrt{2}(1+\exp(\pm ik))(J'+B)$, $F'_{\pm}(k) = J'(1+\exp(\pm ik))$, $G'(k) = -2J'\cos(\frac{1}{2}(f+1)k)$ and $H' = 2(1+B)$. If we consider the two matrices, we notice that the change in the nonlinearity parameter B affects all the off-diagonal elements in $H_{MF}(k)$, whereas, it affects only the first two off-diagonal elements of $H_{comp}(k)$. Hence the two matrices are similar only for very small values of B. The presence of the extra B term in $H_{MF}(k)$ causes the lowering of the eigenvalues corresponding to the off-site breather. Thus the off-site breather appears separate from the continuum band in the mean field case.

To show that the lowest isolated bands in Fig. 1 actually corresponds to the quantum equivalent of the on-site classical discrete breather, we establish their main characteristics, the spatial localization, by calculating the spatial correlation function.

To calculate the spatial correlation function for the on-site discrete breather, we consider the eigenvector $|\alpha\rangle$ (Eq. (12)) that corresponds to the lowest eigenvalue of the Hamiltonian matrix (for complete Hamiltonian, Eq. (2)). Fig. 2(a) and Fig. 2(b) show the spatial correlation function for the on-site discrete breather for the centre and edge of the Brillouin zone respectively. The parameters B and J' are the same as in Fig. 1.(f). From the figure we can see that the spatial correlation function has a large peak at $n - n' = 0$ and is almost zero for other values of $n - n'$. This means that the breather is spatially localized at a single site n, which is a key characteristic of onsite discrete breathers. Fig. 2(c) and 2(d) shows the correlation functions for the mean field Hamiltonian (Eq. (13)). The values of the parameters B and J are same as the values in Fig. 1.(a).

The localization property can also be seen from the plot of the probability

$|C_i|^2$ of the translational invariant states $|\psi_i\rangle$ corresponding to the ground state of the system [18]. Fig. 3(a) and Fig. 3(b) show the plots corresponding to the wavevector k at the center and near the edge of the Brillouin zone respectively. From the figures we notice that at the centre of the Brillouin zone (Fig. 3(a)), the value of $|C_1|^2$ is much greater than elsewhere. This implies that the ground state system prefers to be in the on-site bound states. This corresponds to the 2-on-site breather band $[2, 0, ...]$ plus its cyclic permutations (Eq. (8)). On the other hand, near the edge of the Brillouin zone (Fig. 3(b)), the value of $|C_2|^2$ is much greater than the rest. Hence the system prefers to be in the off-site bound state $[1, 1, 0, ...]$ plus cyclic permutations (Eq. (9)). These results are in agreement with Xin-Guang and Yi [14]. Fig. 3(c) and Fig. 3(d) show the corresponding figures for the mean field Hamiltonian (Eq. (13)) and it shows behavior similar to that for the full Hamiltonian case (Eq. (2)).

6.2. ***Four quanta sector***

So far we have restricted our study to the two-quanta sector. Proceeding in the same way we have generalized the studies to the case of the four-quanta sector, corresponding to the block H_4 of the Hamiltonian matrix. In this case we expect five bands as there are five possibilities of distributing four quantas on f lattice sites. These are $[4, 0, 0, 0, ...]$, $[3, 1, 0, 0, ...]$, $[2, 2, 0, 0, ...]$, $[2, 1, 1, 0, ...]$ and $[1, 1, 1, 1, 0, 0....]$ and their cyclic permutations. Fig. 4 shows the eigenspectra for the complete Hamiltonian (Eq. (2)) for four quanta sector for the attractive interaction $B < 0$ case. Here we have considered 51 lattice sites. From the figure we see that the energy spectrum has the same qualitative behavior as the two-quanta case (Fig. 1(d)) as discussed above. However, here the continuum band splits into other bands. As expected, we can observe 5 bands clearly. The overlap of the 3rd and 4th band as seen in the figure reduces with increase in the strength of nonlinearity parameter B and these two bands gets separated. We have not shown the separated bands here, since for larger value of B, the lowest band splits further away from the other bands and it is difficult to show all the bands in the same figure. The lowest band which is separated by a large magnitude corresponds to the single 4-on-site breather band, $[4, 0, ...]$ plus cyclic permutations (similar to Eq. (8) for the two-quanta case). The next lowest band corresponds to the 3-on-site breather band plus single boson band $[3, 1, 0, ...]$ plus cyclic permutations. The third band is the double 2-on-site breather band $[2, 2, 0, ...]$ plus cyclic permutations, the 4-th band is the 2-on-site breather band plus two

single bosons $[2, 1, 1, 0, ...]$ plus cyclic permutations and 5-th band (top band) consists of only single bosons $[1, 1, 1, 1, 0, ...]$. It is interesting to mention here that these five bands for the 4-quanta sector as mentioned above also occur in the discrete nonlinear Schrodinger (DNLS) model [27].

Fig. 5(a) shows the correlation function for the lowest band (Fig. 4) of the four-quanta sector for 11 lattice sites. From the figure we can see that, as expected for the lowest band at the center of the Brillouin zone ($k/\pi = 0$), the correlation function have a large peak at $n - n' = 0$ and is almost zero for other values of $n - n'$. The large peak corresponds to 4-on-site discrete breather state. Small finite values of the correlation function for non-zero values of $n - n'$ as seen in the figure are due to finite size effect of the lattice. This can be seen from Fig. 5(b) where we have plotted the same correlation function for 51 lattice sites and we can see that most of these peaks at non-zero value of $n - n'$ disappear. Fig. 5(c) shows the correlation function for the next lowest band (Fig. 4) of the four-quanta sector for 11 lattice sites. As mentioned above, this band corresponds to the 3-on-site breather band plus single boson band $[3, 1, 0, ...]$ plus cyclic permutations. From the figure we can see that there is a large peak at $n - n' = 0$ and oscillations of the correlation function which have significant weight even at large values of $n - n'$. The large peak corresponds to 3-on-site discrete breather state and the oscillation corresponds to the one free-phonon state. To show that the oscillation is not a finite size effect, we have calculated the same correlation function for 51 lattice sites as shown in Fig. 5(d). From the figure we can see that the oscillations have significant weight even at $n - n' = 6$.

6.3. ***Two quanta sector with next-nearest neighbour interaction***

We now present the results for the one-dimensional β-FPU lattice with nearest and next nearest neighbor interactions (Eq. (14)). This is topologically equivalent to a zig-zag chain. If the lattice periodicity for the straight chain is a, then for the zig-zag chain it is doubled to $2a$. Accordingly the Brillouin zone boundary for the zig-zag chain is at half its value ($\pi/2a$) as compared to that of the straight chain. Thus the energy spectrum for the one-dimensional β-FPU lattice with NN and NNN interactions is expected to be qualitatively similar to that of the same lattice system with only nearest neighbor interactions (Eq. (2)), except that the Brillouin zone boundary of the NNN will be at half of the value as that of the NN. This is exactly shown in Fig. 6 for the mean field Hamiltonian (Eq. (15)) and in Fig. 7 for the full Hamiltonian (Eq. (14)) for the two-quanta sector. Comparison of Fig. 6

with Fig 1(c) for the mean field case, we see that the nature of the energy spectrum is similar in both cases, and the Brillouin zone boundary in Fig. 6 occurs at exactly half the value of the zone boundary in Fig. 1(c). Comparison of Fig. 7 and Fig. 1(d) also shows similar behavior for the respective full Hamiltonian cases. Fig. 8 (a) and (b) show the plots for the correlation functions calculated for the lowest mode of the eigenvalue spectrum (Fig. 7) at the centre and the edge of the Brillouin zone respectively. This mode corresponds to on-site discrete breather or the on-site bound biphonon state. The peak of the correlation function at a particular site $n - n' = 0$ shows the localization property of the discrete breather. Fig. 8(c) and Fig. 8(d) are the plots of the probability amplitudes at the center and edge of the Brillouin zone respectively. From Fig. 8(c) we can see that there is a large amplitude of $|C_1|^2$, which corresponds to the on-site discrete breather or the on-site bound biphonon mode for $k = 0$. On the other hand at the edge of the Brillouin zone $|C_2|^2$ shows that the 2-off-site bound biphonon state is more probable. Similar behavior is observed for the mean field Hamiltonian (Eq. (15)).

7. Conclusion

In conclusion, we have studied the quantization of the β-FPU lattice with nearest and next-nearest neighbor interactions using boson quantization rules and number conserving approximations. The eigenvalue spectra in the two- and four-quanta sector are obtained using an numerically exact diagonalization technique. From the calculation of the energy spectrum and correlation function of the system, we have shown that the quantum breathers exist as bound states of onsite and nearest sites multi-phonons. We have shown that the probability amplitude of the translational invariant states corresponding to a quantum discrete breather state depends on the wave vector. For the wavevector at the centre of the Brillouin zone, quantum breathers with bound states of onsite multi-phonons are preferred. On the contrary, for the wavevector at the edge of the Brillouin zone, the quantum breathers with bound states of nearest sites multi-phonons are preferred. The inclusion of next-nearest neighbour interactions do not change the nature of the eigenspectra and the correlation functions of the system except that the Brillouin zone is reduced to half.

8. Appendix A:

The bivibron tunneling term $\sum_j (a_j^\dagger)^2 a_j a_{j\pm1}$ can be written as: $\sum_j (a_j^\dagger)^2 a_j a_{j\pm1} = \sum_j a_j^\dagger a_j^\dagger a_j a_{j\pm1} = \sum_j a_j^\dagger a_j^\dagger a_{j\pm1} a_j = \sum_j a_j^\dagger a_{j\pm1} a_j^\dagger a_j$ In the mean field approximation we take out the expectation value of the last two terms. This gives the bivibron tunneling term as $\sum_j (a_j^\dagger)^2 a_j a_{j\pm1} \approx \langle a^\dagger a \rangle (\sum_j a_j^\dagger a_{j\pm1})$.

Similarly, the corresponding h.c. term can be written as: $\sum_j a_{j\pm1}^\dagger a_j^\dagger a_j a_j = \sum_j a_j^\dagger a_{j\pm1}^\dagger a_j a_j = \sum_j a_j^\dagger a_j a_{j\pm1}^\dagger a_j$. Under mean field approximation this term can be written as $\approx \langle a^\dagger a \rangle \sum_j a_{j\pm1}^\dagger a_j$ which for an infinite lattice ($N \to \infty$) can be written as $\langle a^\dagger a \rangle \sum_j a_j^\dagger a_{j\mp1}$.

We now show that $\langle a_j^\dagger a_j \rangle = \langle a^\dagger a \rangle = m$, independent of lattice site j and depends only on the number of quanta m in the state. For this we consider a system with three lattice sites and a state $|\Psi\rangle$ with two quanta ($m = 2$). The state is given by Eq. (10) along with Eq. (8) and Eq. (9).

$$\begin{aligned} a_1^\dagger a_1 |\Psi\rangle &= C_1 a_1^\dagger a_1 |\psi_1\rangle + C_2 a_1^\dagger a_1 |\psi_2\rangle \\ &= C_1 \left(2[2\ \ 0\ \ 0] + 0 + 0\right) + C_2 \left([1\ \ 1\ \ 0] + 0 + t^2[1\ \ 0\ \ 1]\right) \end{aligned}$$

Taking the scalar product with $\langle\Psi|$ and using orthonormality condition for the number states $[2\ \ 0\ \ 0], [0\ \ 2\ \ 0], ..[1\ \ 1\ \ 0]..$, we get

$$\langle\Psi|a_1^\dagger a_1|\Psi\rangle = 2|C_1|^2 + |C_2|^2 + |C_2|^2 = 2(|C_1|^2 + |C_2|^2) = 2$$

Similarly,

$$a_2^\dagger a_2 |\Psi\rangle = C_1 \left(0 + 2t[0\ \ 2\ \ 0] + 0\right) + C_2 \left([1\ \ 1\ \ 0] + t[0\ \ 1\ \ 0] + 0\right)$$

and

$$a_3^\dagger a_3 |\Psi\rangle = C_1 \left(0 + 0 + 2t^2[0\ \ 0\ \ 2]\right) + C_2 \left(0 + t[0\ \ 1\ \ 1] + t^2[1\ \ 0\ \ 1]\right)$$

Taking the scalar product with $\langle\Psi|$, we get

$$\langle\Psi|a_2^\dagger a_2|\Psi\rangle = 2|C_1|^2 + |C_2|^2 + |C_2|^2 = 2(|C_1|^2 + |C_2|^2) = 2$$

and,

$$\langle\Psi|a_3^\dagger a_3|\Psi\rangle = 2|C_1|^2 + |C_2|^2 + |C_2|^2 = 2(|C_1|^2 + |C_2|^2) = 2$$

This shows that $\langle a_j^\dagger a_j\rangle = \langle a^\dagger a\rangle$ is independent of j. To show that $\langle a^\dagger a\rangle$ is independent of f, we consider a system with 5 lattice sites. For the two quanta sector ($m = 2$) and five lattice sites ($f = 5$) we get,

$$\begin{aligned} a_1^\dagger a_1|\Psi\rangle &= C_1(2[2\ \ 0\ \ 0\ \ 0\ \ 0] + 0 + 0 + 0 + 0) + C_2([1\ \ 1\ \ 0\ \ 0\ \ 0] + 0 \\ &+ 0 + 0 + t^4[1\ \ 0\ \ 0\ \ 0\ \ 1]) + C_3([1\ \ 0\ \ 1\ \ 0\ \ 0] + 0 + 0 \\ &+ t^3[1\ \ 0\ \ 0\ \ 1\ \ 0] + 0) \end{aligned}$$

Hence,

$$\langle\Psi|a_1^\dagger a_1|\Psi\rangle = 2|C_1|^2+|C_2|^2+|C_2|^2+|C_3|^2+|C_3|^2 = 2(|C_1|^2+|C_2|^2+|C_3|^2) = 2$$

Similarly $\langle\Psi|a_2^\dagger a_2|\Psi\rangle = \langle\Psi|a_3^\dagger a_3|\Psi\rangle = \langle\Psi|a_4^\dagger a_4|\Psi\rangle = \langle\Psi|a_5^\dagger a_5|\Psi\rangle = 2(|C_1|^2 + |C_2|^2 + |C_3|^2) = 2$. In general, for an arbitrary state $|\Psi\rangle$ with m quanta and f lattice sites $\langle\Psi|a_n^\dagger a_n|\Psi\rangle = m$ for all lattice sites i.e. $n = 1, 2, \ldots, f$.

Acknowledgement: BD would like to thank DST and BCUD-PU for financial assistance through research projects and INSA-RSE for a visiting fellowship. BD would also like to thank Heriot-Watt University, Edinburgh, UK and ICTP, Trieste, Italy for hospitality, where part of the work was done.

References

[1] *Focus issue on the occasion of the fifty years of Fermi-Pasta-Ulam problem* (2005) Chaos 15.

[2] S. Lepri, R. Livi and A. Poloti (2005) Chaos 15 015118; A. Fillipov, B. Hu, B. Li and A. Zeltser (1998) J. Phys. A: Math. Gen. 31 7719; G. Benettin, R. Livi and A. Ponno (2009) J. Stat. Phys. 135 873.

[3] S. Flach and A.V. Gorbach (2008) Phys. Rep. 467 1.

[4] R. S. MacKay and S. Aubry (1994) Nonlinearity 7 1623.

[5] R. Sarkar and B. Dey (2006) J. Phys. A: Math. Gen. 39 L99.

[6] R. Sarkar and B. Dey (2007) Phys. Rev. E 76 016605; R. Sarkar and B. Dey (2007) Eur. Phys. J. Special Topics 147 73 and references therein.

[7] M. J. Ablowitz, D. J. Kaup, A. C. Newell and H. Segur (1973) Phys. Rev. Lett. 30 1262.

[8] N. N. Akhmediev, V. M. Eleonskii, N. E. Kulagin (1987) Theoretical and Mathematical Physics 72 Issue 2 809.

[9] R. Grimshaw, A. Slunyaev and E. Pelinovsky (2010) Chaos 20 013102.

[10] R. F. Dashen, B. Hasslacher and A. Neveu (1974) Phys. Rev. D 10 4114; (1975) *ibid.* 11 3424.

[11] L. D. Faddeev and V. E. Korepin (1978) Phys. Rep. 42 Issue 1 1.

[12] For a review see, R. A. Pinto and S. Flach in Dynamical Tunneling: Theory and Experiment (2011) CRC Press, Eds. S. Keshavamurthy and P. Schlagheck, pp 339-382.

[13] Z. Ivić and G. P. Tsironis (2006) Physica D 216 200.

[14] H. Xin-Guang and T. Yi (2008) Chin. Phys. B 17 4268.

[15] P. S. Riseborough (2012) Phys. Rev. E 85 011129.

[16] H. Xin-Guang *et al.* (2013) Pramana - J. Phys. 81 839.

[17] A. C. Scott, J. C. Eilbeck and H. Gilhøj (1994) Physica D 78 194.

[18] J. C. Eilbeck and F. Palmero (2004) Phys. Letts. A 331 Issue 3-4 201 ; J. Chris Eilbeck, Proceedings of the Third Conference "Localization and Energy Transfer in Nonlinear Systems", June 17-21, San Lorenzo de El Escorial Madrid, eds L. Vzquez, R. S. MacKay, M. P. Zorzano, World Scientific, Singapore, 177–186, 2003

[19] Z. I. Djoufack, A. Kenfack-Jiotsa, J. P. Nguenang and S. Domngang (2010) J. Phys.: Condens. Matter 22 205502.

[20] W. Z. Wang, J. Tinka Gammel, A. R. Bishop and M. I. Salkola (1996) Phys. Rev. Lett. 76 3598.

[21] M. E. Manley *et al.* (2009) Phys. Rev. B 79 134304.

[22] B. I. Swanson *et al.* (1999) Phys. Rev. Lett. 82 3288.

[23] D. A. Dows and V. Schettino (1973) J. Chem. Phys. 58 5009.

[24] F. M. Russell and J. C. Eilbeck (2007) Euro. Phys. Lett. 78 10004.

[25] J. M. Zhang and R. X. Dong (2010) Eur. J. Phys. 31 591.

[26] E. Anderson, Z. Bai, C. Bischof, S. Blackford, J. Demmel, J. Dongarra, J. Du Croz, A. Greenbaum, S. Hammarling, A. McKenney and D. Sorensen (1999) Lapack User's Guide.

[27] J. Dorignac, J.C. Eilbeck, M. Salerno, and A. C. Scott (2004), Phys. Rev. Letts. **93** 025504.

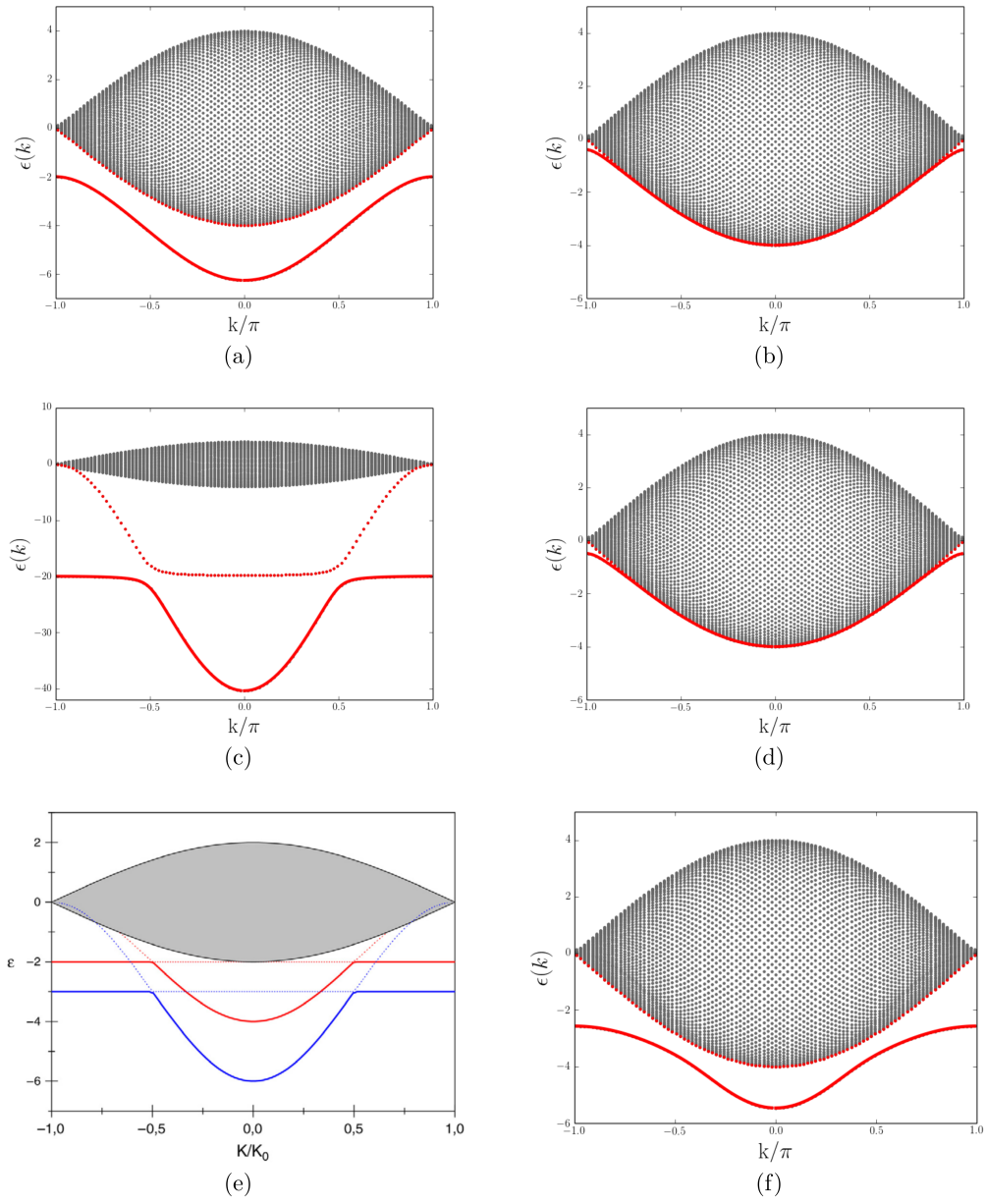

Figure 1: Energy spectrum for(a) Mean field Hamiltonian for $B = -0.2$ and $J = 0.2$ (b) Complete Hamiltonian for $B = -0.2$ and $J' = 1$ (c) Mean field Hamiltonian for $B = -0.2439$ and $J = 0.02439$, (d) Complete Hamiltonian for $B = -0.2439$ and $J' = 1$, (e) Mean Field Results of Ivić and Tsironis, (figure obtained from [13]) (f) Complete Hamiltonian for $B = -1.2857$ and $J' = 1$

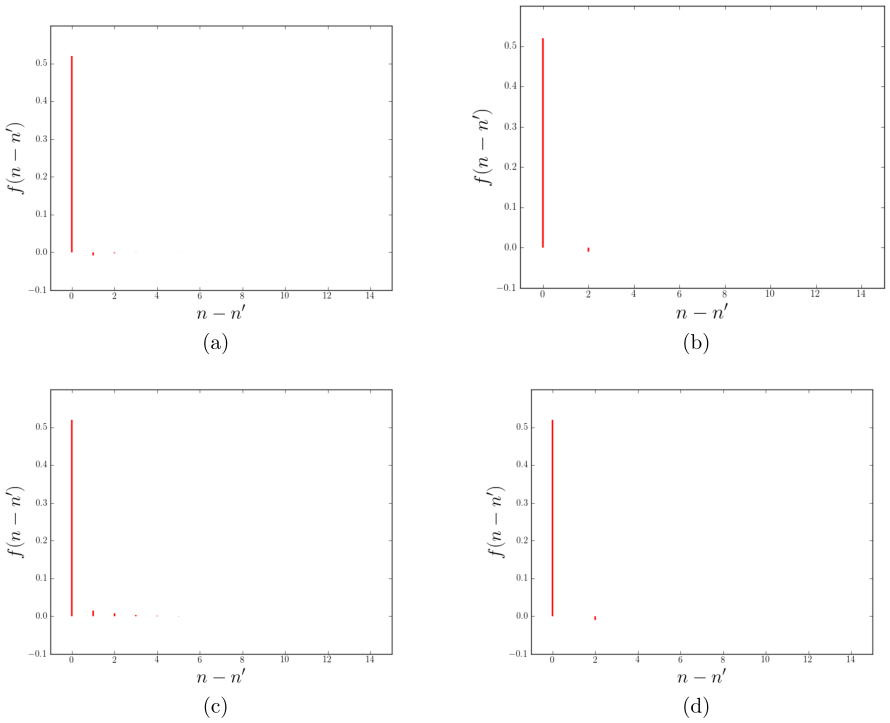

Figure 2: (a)Spatial correlation Function for $k/\pi = 0, B = -1.2857, J' = 1$ for the complete Hamiltonian, (b)Spatial correlation Function for $k/\pi = 50/51, B = -1.2857, J' = 1$ for the complete Hamiltonian, (d) Correlation Function for $k/\pi = 50/51, B = -0.2, J = 0.2$ for the mean field Hamiltonian, (c) Correlation Function for $k/\pi = 0, B = -0.2, J = 0.2$ for the mean field Hamiltonian

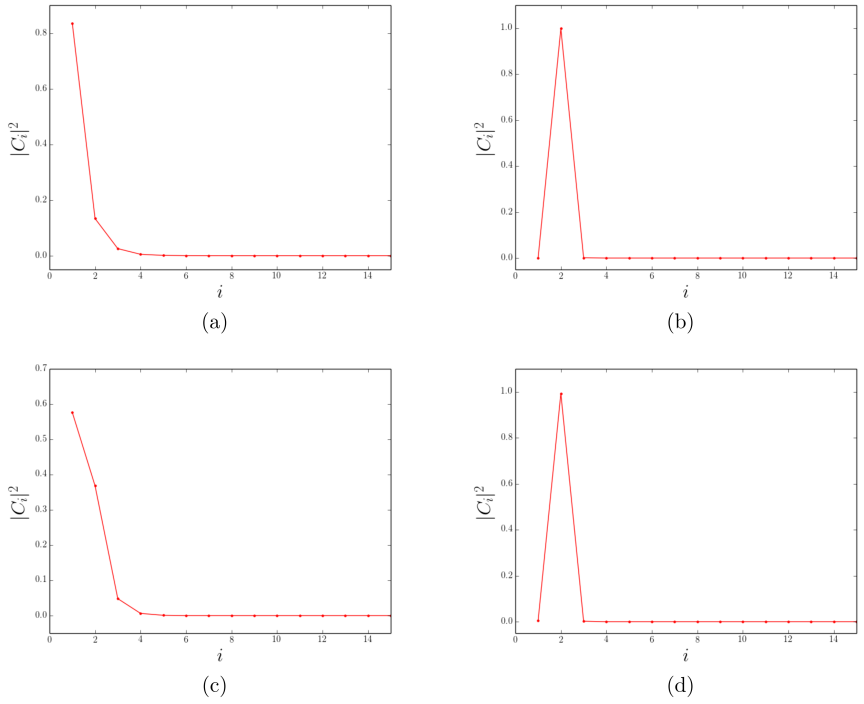

Figure 3: (a) $|C_i|^2$ for $k/\pi = 0, B = -1.2857, J' = 0.07$ for the complete Hamiltonian, (b) $|C_i|^2$ for $k/\pi = 50/51, B = -1.2857, J' = 0.07$ for the complete Hamiltonian, (c) $|C_i|^2$ for $k/\pi = 0, B = -0.2, J = 0.2$, for mean field Hamiltonian, (d) $|C_i|^2$ for $k/\pi = 50/51, B = -0.2, J = 0.2$, for mean field Hamiltonian

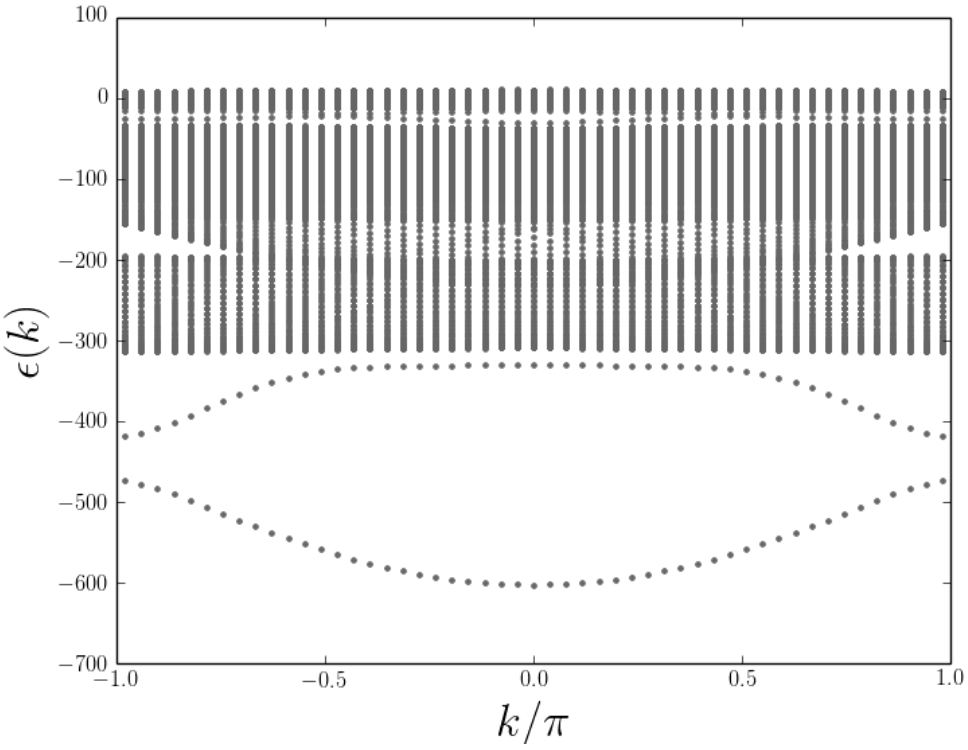

Figure 4: Energy spectrum of the complete Hamiltonian for four quanta, $m = 4$, and 51 sites, $B = -20.0$ and $J' = 1.0$

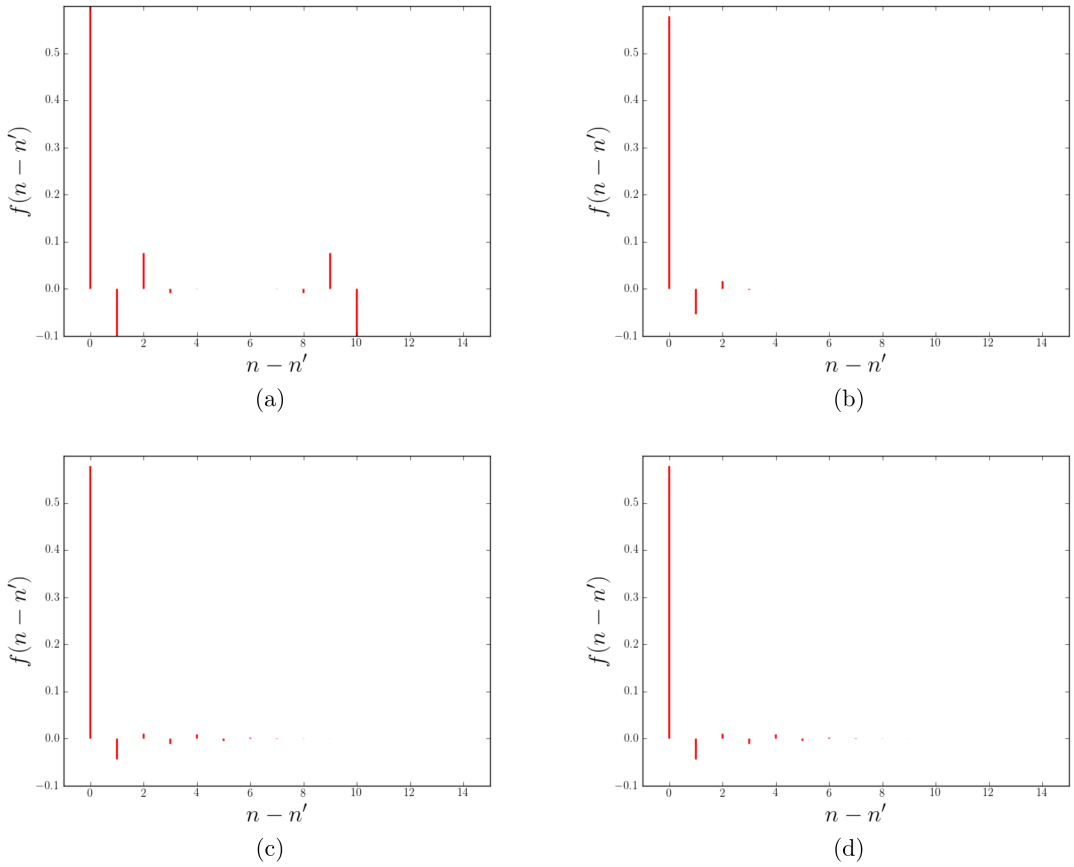

Figure 5: Spatial correlation function for the complete Hamiltonian, for four quanta, $m = 4$, with $k/\pi = 0, B = -20.0$ and $J = 1.0$, (a) for lowest energy mode with 11 sites, (b) for lowest energy mode with 51 sites, (c) for second lowest energy mode with 11 sites, (d) for the second lowest energy mode with 51 sites.

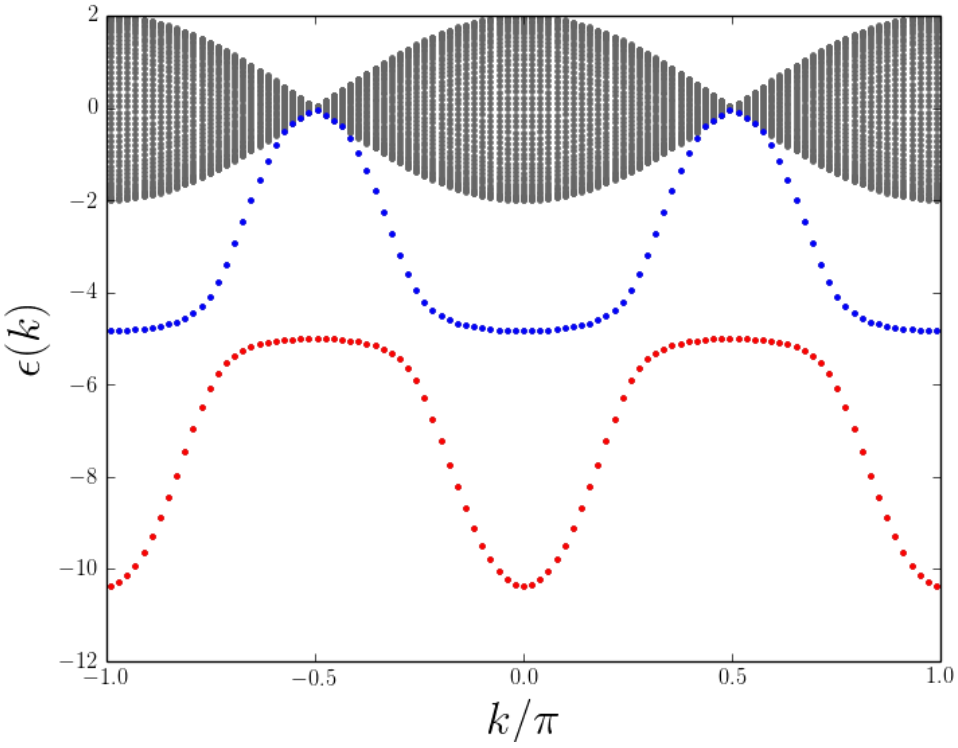

Figure 6: Energy spectrum of the mean field Hamiltonian with nearest and next nearest neighbor interactions for, m=2, $B = -5.0, J = 1, B_1 = -2.5, J_1 = 0.5$, 101 sites

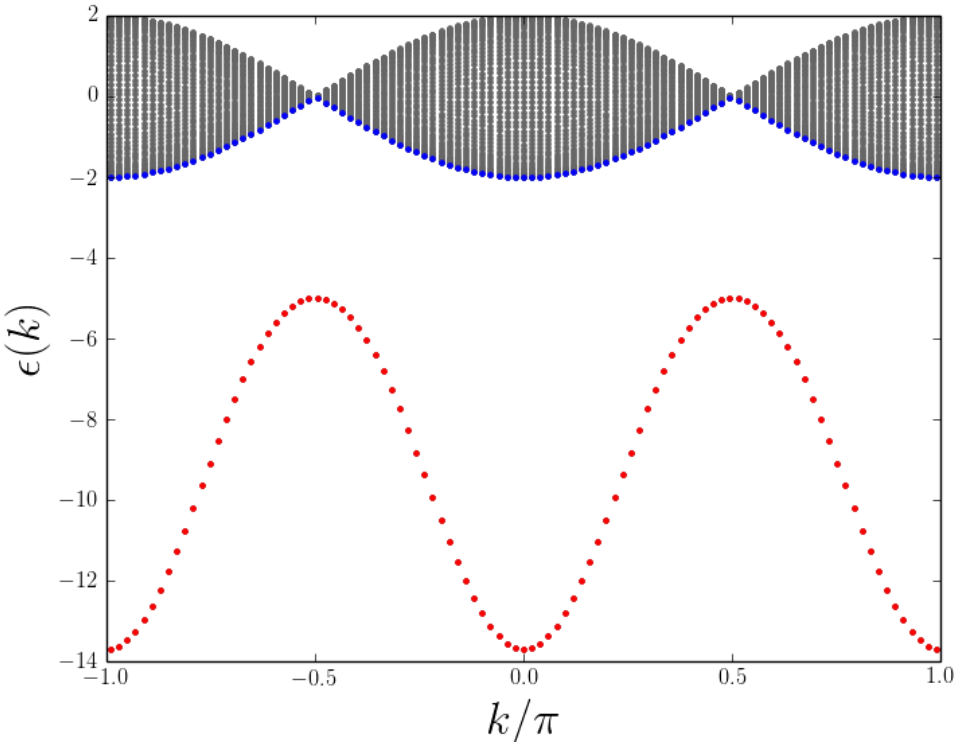

Figure 7: Energy spectrum of the complete Hamiltonian with nearest and next nearest neighbor interactions for, m=2, $B = -5.0, J' = 1, B_1 = -2.5$, $J_1' = 0.5$, 101 sites

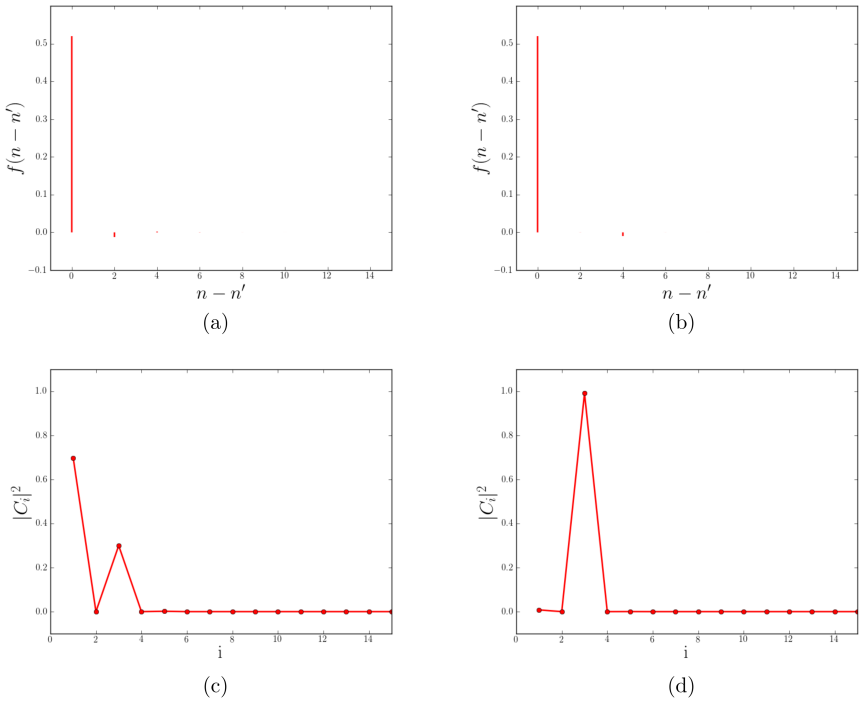

Figure 8: (a) Spatial correlation function for $k/\pi = 0, B = -5.0, J = 1, B_1 = -2.5$ and $J_1 = 0.5$, (b) Spatial correlation function for $k/\pi = 50/51, B = -5.0, J = 1, B_1 = -2.5$ and $J_1 = 0.5$, (c) $|C_i|^2$ for $k/\pi = 0, B = -5.0, J = 1, B_1 = -2.5$ and $J_1 = 0.5$, (d) $|C_i|^2$ for $k/\pi = 50/51, B = -5.0, J = 1, B_1 = -2.5, J_1 = 0.5$ of the complete Hamiltonian with nearest and next nearest neighbor interactions